Acta Crystallographica Section B
Structural Science
ISSN 0108-7681

Charge density of (−)-strychnine from 100 to 15 K, a comparison of four data sets

Marc Messerschmidt, Stephan Scheins and Peter Luger*

Free University Berlin, Institute for Chemistry/Crystallography, Takustrasse 6, 14195 Berlin, Germany

Correspondence e-mail: luger@chemie.fu-berlin.de

Received 21 October 2005
Accepted 13 December 2005

Strychnine has an interesting oligocyclic structure of seven condensed rings. It is easy to crystallize and gives crystals of excellent quality which diffract nicely to high regions in reciprocal space. It was thus chosen for a comparative charge-density study based on four high-resolution data sets ($\sin\theta/\lambda \geq 1.15$ Å^{-1}) that were measured with different experimental setups in the temperature range 100–15 K. In addition, a theoretical charge density was derived from a B3LYP/6-311++G(3df,3pd) calculation. The agreement expressed in bond topological parameters among the four experimental charge densities is better than between experiment and theory.

1. Introduction

The electronic charge density $\rho(\mathbf{r})$ of a chemical structure, which can be obtained from a high-resolution X-ray diffraction experiment at low temperature, can reveal important quantitative information about atomic and bond properties, non-bonding interactions, stability and reactivity. Since the mid-nineties the time-consuming nature of X-ray data collection has been reduced through the introduction of area detectors. This made it possible to perform charge-density studies on larger molecules of biological interest, where the activity can be examined not only from steric but also from electronic properties (Matta & Bader, 2003). Optimum experimental conditions are essential for a charge-density study. In addition to the crystal quality these conditions depend particularly on the choice of primary radiation, the choice of detector (and the corresponding data reduction software) and the choice of cooling device, and hence the data collection temperature.

Here we report on the charge-density determination of (−)-strychnine, making use of four data sets collected on different diffractometers with synchrotron and conventional Mo $K\alpha$ radiation at temperatures of 100, 25 and 15 K. The evaluated electron densities are compared and should provide an estimation of the reproducibility of results from different experiments. In addition, theoretical calculations were performed to compare with the experimental data.

Strychnine has an interesting oligocyclic structure (Fig. 1) and physiologically behaves as an interneuron poison. In lower doses strychnine has previously been used as a doping agent, since it increases muscular activity. It is easy to crystallize and gives excellent crystals which diffract to high resolution and was thus chosen for this comparative study.

Table 1
Bond lengths (Å) of different C—H bonds.

Bond type	Bond distance
C—H at tertiary carbon	1.07
C—H at secondary carbon	1.073
C—H at aromatic carbon	1.084
C—H at olefinic carbon	1.07

2. Experimental

Four different high-resolution data sets were collected using different experimental setups. Three of these data sets, including their spherical refinements, have already been previously discussed (Meserschmidt *et al.*, 2003), but the most important relevant experimental conditions are summarized as follows:

Two data sets, hereafter called APEX and OXFORD, were measured with conventional Mo $K\alpha$ radiation and a nitrogen gas stream cooling at 100 K at the demonstration sites of the companies. Hence, a SMART three-circle diffractometer with APEX CCD area detector, and an EXCALIBUR2 four-circle diffractometer with a SAPPHIRE CCD area detector were used.

The two other data sets, named SYN and HUBER, were measured on comparable Huber four-circle diffractometers (400 mm diameter, offset χ circle) at 15 and 25 K using a closed-cycle helium cryostat. The SYN data were measured with synchrotron radiation (λ = 0.5 Å) at beamline D3 of the Hasylab/DESY (Hamburg, Germany) with a Bruker Smart 1 K area detector. For the HUBER data, standard sealed-tube Mo $K\alpha$ radiation and an APEX detector were used. Four different crystals were used for the four X-ray diffraction experiments. For data collections with conventional Mo $K\alpha$ radiation the crystals were of comparable size (*ca* 0.5 × 0.5 × 0.4 mm), while the synchrotron crystal was smaller with the dimensions 0.3 × 0.3 × 0.2 mm. Similar resolutions ($\sin\theta/\lambda \geq 1.15$ Å^{-1}) were obtained for all data sets.

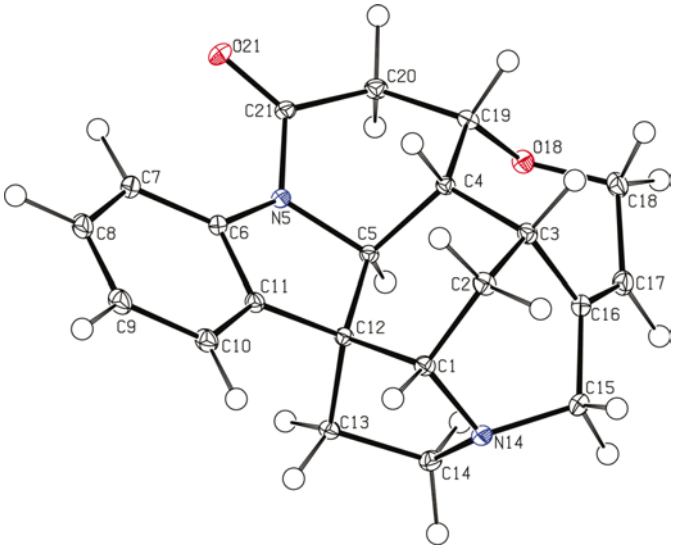

Figure 1
Molecular structure of strychnine in the crystal. *ORTEP*III representation (Burnett & Johnson, 1996) with displacement ellipsoids of the SYN data (measured at 15 K) plotted at 50% probability.

The I/σ ratios for the 25 K laboratory data (HUBER) are almost comparable to those of the synchrotron experiment (SYN). The laboratory data set has 9430 (90%) observed unique reflections compared with 9461 (94%) reflections for the SYN data set, which are reduced to 70% for both 100 K experiments. This reduction is expecially pronounced in the high-order regions. For $\sin\theta/\lambda \geq 1.1$ Å^{-1} only 30% of the reflections could be observed at 100 K, with 80% at 25 K using comparable sealed-tube radiation and 90% at 15 K with synchrotron radiation. This demonstrates how the resolution which can be achieved can be strongly influenced by the measurement temperature. Therefore, not only the maximum resolution, but also the fraction of observed reflections has to be considered as important for such experiments.

3. Multipole refinements

The X-ray structure of strychnine has been previously determined at 133 K by Mostad (1985). A first spherical refinement was performed with *SHELXL* (Sheldrick, 1997). The Hansen–Coppens multipole formalism (Hansen & Coppens, 1978) as implemented in the *XD* program system (Koritsánszky *et al.*, 1995) was then applied for aspherical refinement of all data sets. The atomic electron density $\rho_a(\mathbf{r})$ in this model constructed from spherical harmonics is

$$\rho_a(\mathbf{r}) = \rho_{\rm core}(r) + P_v\kappa^3\rho_{\rm val}(\kappa r) + \sum_{l=0}^{l_{\rm max}} \kappa'^3 R_l(\kappa'\mathbf{r}) \sum_{m=0}^{1} P_{lm\pm} y_{lm\pm}(\theta,\varphi), \quad (1)$$

where the first two terms represent the spherical core and valence density, and the last term accounts for aspherical contributions. In all cases the full-matrix *LSQ* program (*XDLSM*) of the *XD* (Koritsánszky *et al.*, 1995) package was used with statistical weights

$$w_H = \sigma^{-2}(F_{\rm obs}(\mathbf{H})). \quad (2)$$

A stepwise procedure was used in the refinement. C, N and O atoms were refined up to the hexadecapole level, while for H atoms only a bond-directed dipole was refined. Hydrogen-bond distances were fixed at neutron distances (Allen *et al.*, 1992) according to their bond type (Table 1).

According to the different hybridizations and atom types, altogether seven κ's were introduced. For H atoms a fixed κ of 1.2 was used, while all other κ parameters were refined. For κ' energy-optimized values were used. The resulting agreement factors for the four data sets are summarized in Table 2.

The HUBER 25 K laboratory data set has the smallest $R_{\rm int}$ value and could be refined to the lowest reliability factors with the multipole formalism. From this comparison this data set is even slightly better than the synchrotron data set. Altogether all data sets are of comparable quality, however, the low GoF's for the APEX and OXFORD data sets suggest that the σ

Table 2
Summary of experimental data and the results of the multipole refinement.

	APEX	OXFORD	SYN	HUBER
Temperature (K)	100	100	15	25
Crystal volume (mm^3)	0.10	0.10	0.02	0.11
Resolution ($\sin\theta/\lambda$) ($Å^{-1}$)	1.22	1.21	1.18	1.15
Completeness (%)	92.0	91.4	84.8	92.4
No. of reflections	128 444	76 554	40 614	85 918
No. of unique reflections	11 937	11 615	10 034	10 475
No. of reflections $>2\sigma$	8480	8192	9461	9430
Redundancy	10.8	6.6	4.0	8.2
R_{int} (%)	4.7	2.8	3.5	2.5
$R(I>2\sigma)$	0.017	0.023	0.020	0.017
R_{multi}(all)	0.026	0.037	0.023	0.021
R_w	0.018	0.016	0.021	0.018
GoF	0.47	0.69	1.2	0.93
N_{ref}/N_{var}	9.2	8.9	10.3	10.2

values which were entered into the weighting scheme might not have been properly scaled.

4. Theoretical calculations

Theoretical calculations were performed with the B3LYP density functional using the *GAUSSIAN* program (Frisch *et al.*, 1998). A geometry optimization with 6-31G(d,p) basis set led to a slightly different geometry with a maximum deviation below 0.1 Å for heavy atoms and 0.2 Å for H atoms and is therefore not further discussed. A single point calculation was performed with 6-311++G(3df,3pd) at the experimental geometry and allows a direct comparison of the theoretical topological parameters with the experimental values. The topological analysis was performed with *Morphy*98 (Popelier & Bone, 1998).

5. Results and discussion

5.1. Strychnine structure

The redetermined structures at 100, 25 and 15 K do not differ markedly from that described by Mostad at 133 K; the major differences being the displacement parameters at 25 and 15 K. While for the 100 K data sets the U_{eq} values vary between 0.01 and 0.025 $Å^2$, there is a distinct decrease in the thermal parameters when the temperature drops to 15 K by at least a factor of two (for details see Meserschmidt *et al.*, 2003). Hence, data collection for a charge density work seems preferable at the lowest temperature which is feasible.

The molecular structure of strychnine consists of seven condensed rings. Except for the planar phenyl ring, the other rings are non-planar with unusual ring conformations in parts, which reduce the total strain in the oligocyclic ring system. The ring system includes two ternary N atoms and one O atom, as well as one aromatic ring, one double bond and a keto group beside the carbon–carbon single bonds (see Fig. 1).

Table 3
Residual densities (e $Å^{-3}$).

	APEX	OXFORD	SYN	HUBER
Maximum, all data	0.16	0.15	0.25	0.24
Minimum, all data	−0.13	−0.18	−0.20	−0.16
RMS, all data	0.028	0.034	0.042	0.034
Maximum, data up to 1.0 $Å^{-1}$	0.15	0.13	0.20	0.19
Minimum, data up to 1.0 $Å^{-1}$	−0.11	−0.15	−0.14	−0.11
RMS, data up to 1.0 $Å^{-1}$	0.025	0.030	0.036	0.028
Maximum, data up to 0.9 $Å^{-1}$	0.13	0.12	0.18	0.15
Minimum, data up to 0.9 $Å^{-1}$	−0.10	−0.11	−0.13	−0.10
RMS, data up to 0.9 $Å^{-1}$	0.024	0.026	0.033	0.026

5.2. Residual density

The residual density, being the Fourier transform of the $F_o - F_c$ differences, can be utilized as a criterion for the accuracies of the different experiments and the reliability of the multipole model. Usually, selected molecular planes are considered for this purpose; however, because of the spatial geometry of this molecule a three-dimensional distribution of the residual density was calculated and the main results are shown in Table 3.

For all four experiments the maximum residual density is satisfactory at ≤ 0.25 e $Å^{-3}$ if all the data contribute to the Fourier summation; however, it decreases, as expected, if the resolution is lowered. It should be noted that for the 15 and 25 K experiments (SYN and HUBER data) a slightly higher noise level is observed. Compared with the 100 K experiments the SYN and HUBER data sets are those having the highest I/σ ratios and hence the highest number of observed reflections in the high-order region. Therefore, an effective resolution, that means the amount of observed reflections should be taken into account, obviously has an important influence on the residual density.

5.3. Deformation density

The static deformation density allows a first qualitative view of the aspherical density. As an example the plane including the carbonyl group is shown in Fig. 2. All the expected bonding features are clearly visible. The oxygen lone pairs are found to be aligned slightly out-of-plane for all data sets.

5.4. Topological parameters

The topological analysis of $\rho(\mathbf{r})$ was performed using the *XDPROP* part of the *XD* program (Koritsánszky *et al.*, 1995). All the bond critical points (b.c.p.'s) were located. Their most important bond topological parameters are summarized in Table 4.

It is found from the comparison that among the four data sets all comparable bonds have similar values for $\rho(\mathbf{r})$, with small differences mostly for carbon–carbon bonds. With a reliability factor defined as

$$R\rho_i = \sum |\rho_i - \rho_{mean}| / \sum \rho_{mean}, \quad i = 1, .., 4, \qquad (3)$$

agreement between the four data sets can be analyzed. This results in a maximum $R\rho_i$ of 0.028 for SYN data, while the

other possible experimental comparisons agree more closely (see bottom of Table 4).

If the experimental mean values are compared with the theoretical calculation a good agreement is generally found, but at 0.047 the $R\rho$ (between experimental mean and theory) is higher than for any of the experiments. For polar bonds the deviations are larger, especially for C—O bonds. If only C—C bonds are included in the $R\rho$ calculation it reduces to 0.033. This is in line with the experimental deviations, but altogether the experiments compare more favourable with one another than with theory, which could be attributed to the crystal-field or basis-set differences.

The Laplacian $\nabla^2\rho_{\rm bcp}$ shows a larger variation as the second derivative of the charge density. If we perform an analogous comparison as before, $R_i\nabla^2$ of up to 0.137 is obtained (hence also the highest for SYN data), while again the other possible experimental comparisons give markedly lower values below 0.10. As for ρ, the value of $R\nabla^2$ is highest between experi-

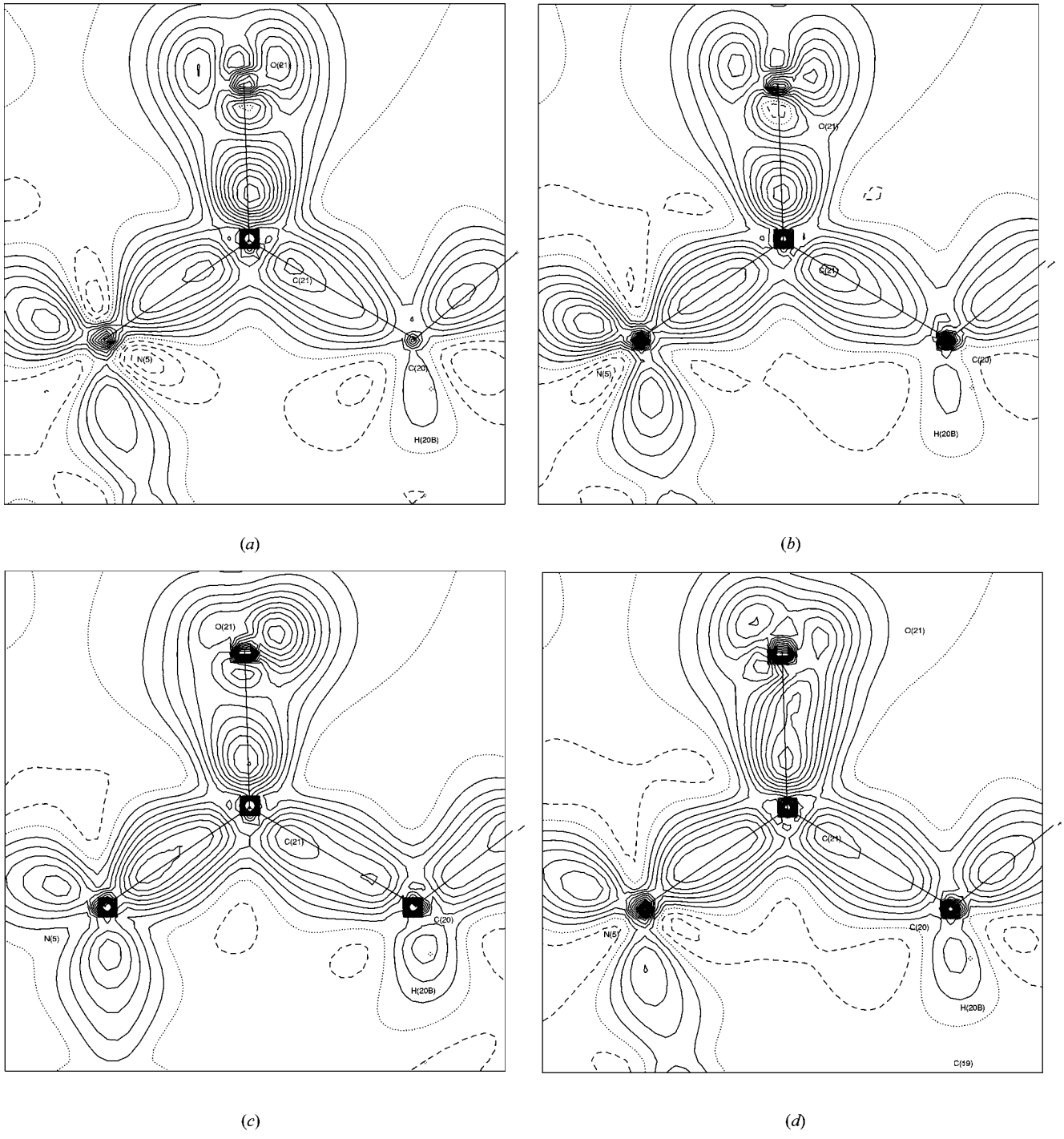

Figure 2
Static deformation density for the N5—C21—C2 plane, containing the carbonyl group. The contours are at 0.1 e Å^{-3}; positive: solid lines, zero: dotted, negative: dashed.

Table 4
Topological parameters of bond critical points.

For the Laplacian only the experimental means are given; the individual values have been deposited.

	Length (Å) (HUBER)	ρ_{bcp} (e Å^{-3})						$\nabla^2\rho_{bcp}$ (e Å^{-5})	
		APEX	OXFORD	SYN	HUBER	Mean	Theo	Mean	Theo
O18—C18	1.4338 (6)	2.08 (4)	1.93 (4)	1.85 (6)	2.00 (3)	1.96 (9)	1.73	−16.5 (19)	−13.3
O18—C19	1.4319 (5)	2.00 (4)	1.89 (4)	1.82 (6)	1.93 (3)	1.91 (7)	1.71	−14.7 (13)	−13.1
O21—C21	1.2301 (6)	3.28 (5)	3.01 (5)	3.08 (7)	3.21 (4)	3.15 (12)	2.78	−37.0 (33)	−15.6
N5—C5	1.4891 (5)	1.76 (3)	1.72 (3)	1.76 (5)	1.73 (3)	1.74 (2)	1.70	−8.6 (9)	−15.4
N5—C6	1.4156 (5)	2.13 (4)	2.10 (4)	2.13 (5)	2.11 (3)	2.12 (1)	1.95	−18.6 (25)	−19.9
N5—C21	1.3747 (5)	2.39 (4)	2.34 (4)	2.48 (6)	2.37 (3)	2.40 (6)	2.16	−23.8 (33)	−23.1
N14—C1	1.4952 (5)	1.86 (3)	1.79 (3)	1.79 (5)	1.83 (3)	1.82 (3)	1.72	−12.9 (6)	−15.0
N14—C14	1.4766 (5)	1.85 (4)	1.85 (4)	1.82 (5)	1.88 (3)	1.85 (2)	1.77	−12.3 (8)	−16.2
N14—C15	1.4715 (5)	2.01 (4)	1.90 (4)	1.82 (5)	1.92 (3)	1.91 (7)	1.79	−12.2 (20)	−16.5
C1—C2	1.5238 (5)	1.79 (3)	1.73 (3)	1.74 (5)	1.74 (3)	1.75 (2)	1.70	−12.7 (15)	−14.5
C1—C12	1.5477 (5)	1.67 (3)	1.64 (3)	1.59 (5)	1.69 (3)	1.65 (4)	1.63	−10.7 (11)	−13.2
C2—C3	1.5359 (5)	1.66 (3)	1.63 (3)	1.64 (5)	1.73 (3)	1.66 (4)	1.65	−10.4 (12)	−13.7
C3—C4	1.5385 (5)	1.68 (3)	1.64 (3)	1.63 (5)	1.72 (2)	1.67 (4)	1.63	−10.3 (15)	−13.2
C3—C16	1.5238 (5)	1.81 (3)	1.71 (3)	1.71 (5)	1.80 (3)	1.76 (5)	1.69	−11.1 (9)	−14.3
C4—C5	1.5374 (5)	1.70 (3)	1.68 (3)	1.74 (5)	1.72 (2)	1.71 (2)	1.67	−11.2 (9)	−13.8
C4—C19	1.5374 (5)	1.78 (3)	1.74 (3)	1.59 (5)	1.82 (3)	1.73 (9)	1.68	−14.1 (31)	−14.2
C5—C12	1.5579 (5)	1.66 (3)	1.61 (2)	1.58 (5)	1.69 (2)	1.64 (4)	1.61	−10.6 (8)	−12.8
C6—C7	1.3996 (5)	2.23 (3)	2.17 (3)	2.02 (6)	2.19 (3)	2.15 (9)	2.14	−15.4 (22)	−22.1
C6—C11	1.4014 (5)	2.27 (3)	2.21 (3)	2.29 (5)	2.25 (3)	2.25 (3)	2.13	−21.5 (10)	−22.2
C7—C8	1.4036 (7)	2.23 (4)	2.18 (4)	2.29 (6)	2.23 (3)	2.23 (4)	2.10	−20.6 (16)	−21.5
C8—C9	1.3991 (7)	1.94 (6)	2.05 (6)	2.26 (6)	2.21 (4)	2.12 (14)	2.11	−15.3 (61)	−21.8
C9—C10	1.4014 (6)	2.23 (4)	2.16 (4)	2.08 (6)	2.17 (3)	2.16 (6)	2.11	−14.7 (10)	−21.9
C10—C11	1.3896 (5)	2.19 (4)	2.20 (4)	2.27 (6)	2.25 (3)	2.23 (3)	2.14	−19.5 (34)	−22.3
C11—C12	1.5076 (5)	1.84 (3)	1.75 (3)	1.79 (5)	1.80 (3)	1.79 (3)	1.75	−12.6 (7)	−15.3
C12—C13	1.5452 (5)	1.75 (3)	1.63 (3)	1.62 (5)	1.71 (2)	1.68 (6)	1.61	−10.2 (10)	−12.9
C13—C14	1.5288 (5)	1.79 (3)	1.71 (3)	1.76 (5)	1.80 (3)	1.77 (3)	1.68	−13.0 (16)	−14.3
C15—C16	1.5098 (6)	1.83 (3)	1.80 (3)	1.82 (5)	1.84 (3)	1.82 (1)	1.75	−13.9 (16)	−15.5
C16—C17	1.3425 (6)	2.38 (4)	2.41 (4)	2.47 (6)	2.43 (3)	2.42 (3)	2.35	−21.6 (24)	−25.8
C17—C18	1.5083 (6)	1.85 (3)	1.83 (3)	1.89 (5)	1.86 (3)	1.86 (2)	1.76	−16.0 (12)	−15.9
C19—C20	1.5470 (5)	1.78 (3)	1.71 (3)	1.65 (5)	1.74 (2)	1.72 (5)	1.63	−13.2 (27)	−13.4
C20—C21	1.5175 (6)	1.81 (3)	1.77 (3)	1.78 (5)	1.82 (3)	1.80 (2)	1.74	−13.2 (11)	−15.4
$R\rho$		0.023	0.016	0.028	0.015		0.047		
$R\nabla^2$		0.097	0.064	0.137	0.062		0.220		

mental mean and theory and again this quantity reduces remarkably (from 0.220 to 0.152) if only the C—C bonds are considered.

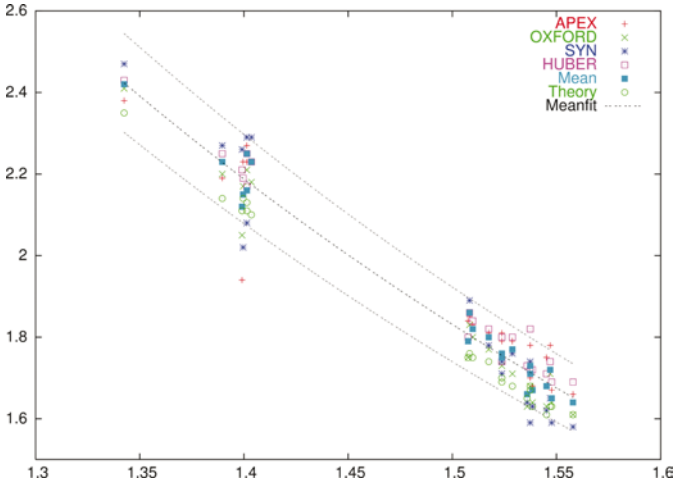

Figure 3
ρ_{bcp} values (e Å^{-3}) for the C—C bonds plotted against the bond lengths (Å). Data are fitted by an exponential function (middle curve). The outer lines are 5% error curves.

From the above-mentioned considerations it can be concluded that the electron density itself at the bond critical points is a very reliable and therefore comparable topological quantity, while the Laplacians should be compared with a much larger standard uncertainty. The maximum error in density can be estimated to within 5%, which is in agreement with previous results, for example, in amino acids, where a large number of measurements could be compared (Flaig *et al.*, 2002; Lecomte *et al.*, 1992).

On the basis of the experimental ρ_{bcp} values (Table 4) the bond strengths can be discussed. For the C—O bonds it is clear that there is significantly higher electron density on the bond critical point of the double bond to the keto oxygen than on the two single bonds originating from O18. For N—C the two N5—C6 and N5—C21 bonds connecting the keto group with the phenyl ring are strongest compared with the other N—C single bonds. The large number of C—C bonds can easily be grouped into three categories:

(i) the double bond C16–C17 with an experimental ρ_{bcp} mean of 2.42 (3) e Å^{-3} as the strongest,

(ii) followed by the six aromatic bonds in the phenyl ring with ρ_{bcp} ranging from 2.12 to 2.25 e Å^{-3}

(ii) and the 15 formal single bonds as the weakest with ρ_{bcp} ranging from 1.64 to 1.86 e Å^{-3}.

An illustration of the entire ρ_{bcp} distribution for the C—C bonds, depending on the bond lengths, is given in Fig. 3. As expected, the least-squares line through the distribution is very close to a linear function. For all four data sets almost all ρ_{bcp} values are found within the 5% error curves, indicating again that this can be considered as the range where the variation of the ρ_{bcp} values has to be taken into account.

5.5. Electrostatic potential

If the electrostatic potential (ESP) of a molecule is examined, the polarization of the total electron density into some regions of a molecule is visible. With a graphical representation of the negative electrostatic potential, reaction sites according to electrophilic attack can be seen. In large biolo-

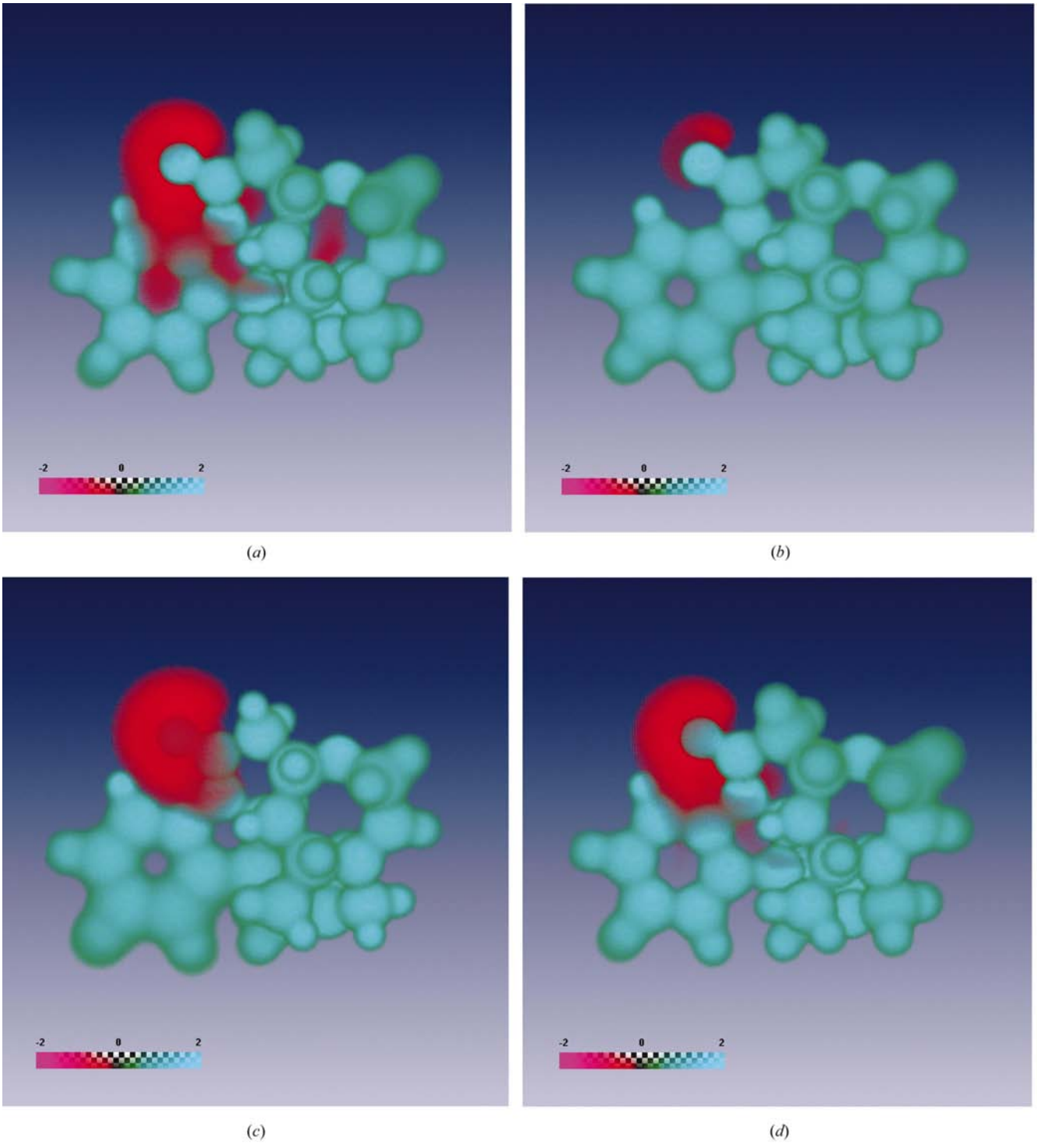

Figure 4
Electrostatic potential in strychnine as a volume-rendering representation. The colour code scale corresponds to values in e Å^{-1}.

gical systems attractive forces of ligands and receptors caused mainly by their ESP should play an important role in the recognition process. We evaluated the ESP using the method of Su & Coppens (1992).

The full distribution of the ESP in space is represented by a volume-rendering technique (see Fig. 4), which uses a colour code in combination with the transparency to make the full three-dimensional information visible (MacDoughal & Henze, 2001). The colour corresponds to the magnitude, while the transparency increases with decreasing magnitude and highlights this way the more important features of the ESP. Owing to the unstructured nature of the positive ESP, only the negative ESP is discussed further, which agrees with chemical intuition for the studied strychnine. Surprisingly, here the difference between the OXFORD and the other three ESP's seems to be significant. The comparison of the three data sets, which were measured with Bruker detectors and where integration and data reduction were performed in nearly the same way, resulted in a very comparable distribution with just slight differences in the expansion of the negative ESP at low values, which can serve as an error estimate. On the other hand, the OXFORD ESP shows a very small negative region at the carbonyl oxygen (see Fig. 4).

The difference of the OXFORD ESP cannot be explained at the moment, but integration software differences cannot be ruled out. Any influence of the measurement temperature is small if present. Also, the monopole charges derived for the four data sets (see supplementary data[1]) gave no clear indication of this difference. The four values for an individual atom generally agree to within two standard uncertainties, however, in line with the observed small negative region in the OXFORD ESP, the monopole charge of O21 is somewhat smaller for this data set compared with the average of the three other data sets [6.35 (4) *versus* 6.49 (7)]. Finally, it should be mentioned that strychnine with no polar groups except for the keto group should not show large polarizations.

6. Conclusions

Four high-order data sets were measured with different setups in the temperature range 100–15 K, using open-flow nitrogen gas stream devices and a closed-cycle helium cryostat. All data sets were of good quality, allowing a refinement of the charge density; the 15 and 25 K data sets have higher I/σ ratios, especially in the high-order region.

A comparison of all bond topological parameters shows good agreement. The experimental findings agree somewhat better with one another than with the results from a theoretical calculation. The observed deviations for ρ are below 5%, but $\nabla^2\rho$ shows a much higher variation. For the ESP a distinct difference between the OXFORD and the other three data sets is observed.

Finally, within the small variation for the well diffracting strychnine crystal, the laboratory data set measured at 25 K has the best quality. Even the number of observed reflections is nearly as good as for the synchrotron data set measured at 15 K, but with a much smaller crystal for the last one.

In general, the lowest possible temperature should be used for charge-density determinations of organic compounds to obtain the optimum I/σ ratios. For small crystals synchrotron radiation could be an essential addition.

The authors thank Bruker AXS, Oxford Diffraction Ltd and the Hasylab (DESY) for providing instrument time. This work was funded by grants from the DFG (grant Lu 222/24-1 and 24-3) which are gratefully acknowledged.

References

Allen, F. H., Kennard, O., Watson, D., Brammer, L., Orpen, A. & Taylor, R. (1992). *International Tables for Crystallography*, Vol. C, ch. 9.5, pp. 685–706. Dordrecht: Kluwer Academic Publishers.
Burnett, M. N. & Johnson, C. K. (1996). *ORTEP*III. Report ORNL-6895. Oak Ridge National Laboratory, Tennessee, USA.
Flaig, R., Koritsanszky, T., Dittrich, B., Wagner, A. & Luger, P. (2002). *J. Am. Chem. Soc.* **124**, 3407–3417.
Frisch, M. J. *et al.* (1998). *GAUSSIAN*98, Revision A.7. Gaussian Inc., Pittsburgh, PA, USA.
Hansen, N. K. & Coppens, P. (1978). *Acta Cryst.* A**34**, 909–921.
Koritsánszky, T., Howard, S., Richter, T., Su, Z. W., Mallinson, P. R. & Hansen, N. K. (1995). *XD*. Freie Universität, Berlin, Germany.
Lecomte, C., Ghermani, N., Pichon-Pesme, V & Souhassou, M. (1992). *J. Mol. Struct. (Theochem.)* **255**, 241–260.
MacDoughal, P. J. & Henze, C. E. (2001). *Theoret. Chem. Acc.* **105**, 345–353.
Matta, C. F. & Bader, R. F. W. (2003). *Proteins Struct. Funct. Genet.* **52**, 360–399.
Meserschmidt, M., Meyer, M. & Luger, P. (2003). *J. Appl. Cryst.* **36**, 1452–1454.
Mostad, A. (1985). *Acta Chem. Scand. B*, **39**, 705–716.
Popelier, P. & Bone, R. (1998). Technical Report. UMIST, Manchester, UK.
Sheldrick, G. M. (1997). *SHELXL*97. University of Göttingen, Germany.
Su, Z. & Coppens, P. (1992). *Acta Cryst.* A**48**, 188–197.

[1] Supplementary data for this paper are available from the IUCr electronic archives (Reference: LC5019). Services for accessing these data are described at the back of the journal.